Clay Minerals (2002) **37**, 617–628

Dedicated to Prof. Dr. U. Schwertmann on the occasion of his 75th birthday

The influence of octahedral and tetrahedral cation substitution on the structure of smectites and serpentines as observed through infrared spectroscopy

J. BISHOP[1,*], E. MURAD[2] AND M. D. DYAR[3]

[1] *SETI Institute/NASA-Ames Research Center, Moffett Field, CA 94035, USA,* [2] *Bayerisches Geologisches Landesamt, Leopoldstrasse 30, D-95603 Marktredwitz, Germany, and* [3] *Department of Earth and Environment, Mount Holyoke College, South Hadley, MA 01075, USA*

(*Received 29 June 2001; revised 14 November 2001*)

ABSTRACT: Analysis of the near-infrared (NIR) spectral bands of phyllosilicates, together with the mid-infrared bands, enables testing and confirmation of band assignments for the structural OH vibrations. Spectral analyses of selected smectites and serpentine-kaolin minerals are presented here. The results of this study indicate that dioctahedral smectites may contain both in-plane and out-of-plane OH-bending vibrations, as suggested by Farmer (1974). In-plane bands occur near 800–915 cm^{-1}, while the weaker out-of-plane vibrations occur near 600–700 cm^{-1} and are enhanced in dioctahedral smectites when the structure is disrupted by substitutions. Analysis of the OH-stretching vibrations and their NIR overtone bands is also presented for both smectites and serpentine-kaolin minerals. These overtones are more straightforward for serpentines than for kaolinite, and a strong overtone associated with the kaolinite OH-stretching band at 3620 cm^{-1} is found that supports its assignment as an OH-stretching band.

KEYWORDS: infrared spectroscopy, smectites, serpentines, kaolinite, structural OH.

Phyllosilicates and iron oxides/oxyhydroxides are thought to be components of Martian surface material because they are alteration products of basalts that are ubiquitous on the Red Planet (e.g. Bell, 1996; Bishop & Murad, 1996; McSween & Keil, 2000; Bishop *et al*., 2002). Characterization of iron oxides/oxyhydroxides on Earth continue to be important in efforts to identify them on Mars (Cornell & Schwertmann, 1996; Schwertmann & Cornell, 2000). Careful measurement and thoughtful interpretation of the infrared (IR) spectra of these important clay minerals may be critical to interpretation of remotely-sensed data from the Earth and Mars.

The IR spectra of phyllosilicates have been summarized by Farmer (1974). In addition to defining a number of well-characterized OH-stretching and bending vibrations for specific classes of clay minerals, Farmer (1974) noted some IR effects that could not be readily explained, i.e. the OH-stretching bands in kaolinite and the OH-bending bands for some smectites. The objective of this study was to characterize the IR features due to OH in smectite and serpentine clay minerals in more detail by comparing the NIR

* E-mail: jbishop@mail.arc.nasa.gov
DOI: 10.1180/0009855023740064

combination and overtone bands of the OH-stretching and bending vibrations with the corresponding fundamental vibrations in the mid-IR. For phyllosilicates, the OH-stretching (OH_v) bands for the octahedral sheets usually occur in the range 3500–3700 cm^{-1} depending on the type of octahedral cations and structural disorder (Farmer, 1974). Structural OH-bending (OH_δ) vibrations are reported across a wide range for the phyllosilicates including 600–770 cm^{-1} for many trioctahedral minerals and 800–940 cm^{-1} for many dioctahedral minerals (Farmer, 1974).

Infrared spectra of serpentine-kaolin minerals

The mid-IR spectral features of kaolinite are summarized by Farmer (1974) and four distinct OH groups have been identified for kaolinite (Bish, 1993). The in-plane OH_δ vibrations are observed at 936 cm^{-1} for surface OH groups and at 915 cm^{-1} for inner OH groups; additional bands near 701 and 755 cm^{-1} are associated with the surface hydroxyls (Farmer, 1974). Four OH_v vibrations are observed near 3697, 3670, 3652 and 3620 cm^{-1} in well-ordered kaolinites (Farmer, 1998). The strong band at 3697 cm^{-1} is assigned to the in-phase vibration and the weak bands near 3670 and 3652 cm^{-1} are assigned to anti-phase vibrations of the inner surface hydroxyls (Farmer, 1974). Fe-bearing kaolinites exhibit bands due to AlFeOH bending at 865–875 cm^{-1} and stretching at 3607 cm^{-1} (Mendelovici *et al*., 1979). The NIR bands for kaolinite include a triplet at 1.395, 1.405 and 1.415 μm (7160, 7120, 7070 cm^{-1}) due to overtones of the OH_v vibrations and a doublet at 2.16 and 2.20 μm (4630, 4545 cm^{-1}) due to combinations ($OH_{v+\delta}$) of the OH-stretching and bending fundamentals (Clark *et al*., 1990).

Serpentines such as chrysotile and antigorite exhibit OH-stretching bands in the range 3650 to 3700 cm^{-1} and OH_δ bands due to inner and surface hydroxyls near 618 and 646 cm^{-1} (Farmer, 1974). Distinguishing between the inner and outer OH groups is not possible and these bands are often complicated by substitution of Al for Mg in the octahedral sites and Al for Si in the tetrahedral sites (Farmer, 1974). The NIR bands for serpentines occur near 1.35–1.45 μm (~7200 cm^{-1}) due to overtones of the Mg-OH_v vibrations and near 2.3 μm (~4300 cm^{-1}) due to combinations of the Mg-OH stretching and bending fundamentals (King & Clark, 1989).

Infrared spectra of smectites

The mid-IR spectral features of smectites include OH-stretching bands that occur near 3630 cm^{-1} for montmorillonite, and are observed at higher frequencies in Mg-rich smectites and at lower frequencies in nontronites (e.g. Farmer, 1974). Structural OH_δ vibrations have been observed for specific pairs of octahedral cations: ~920 cm^{-1} for Al_2OH, ~880 cm^{-1} for AlFeOH and ~850 cm^{-1} for AlMgOH in montmorillonite; near 818 cm^{-1} for Fe_2OH in nontronite; and at 655 cm^{-1} for Mg_2OH in hectorite (Stubican & Roy, 1961a; Farmer, 1974). More recent studies have examined the influence of octahedral cations on the OH_v (e.g. Madejová *et al*., 1994) and OH_δ (Vantelon *et al*., 2001) bands in smectites and observed specific M_1M_2OH vibrations depending on the octahedral cations (*M*: Al, Fe, Mg). The NIR bands due to the OH_v overtone are observed at 7090 cm^{-1} (1.41 μm) for montmorillonite, at ~7050 cm^{-1} (1.42 μm) for nontronite, and as a doublet near 7190 cm^{-1} (1.39 μm) for hectorite. NIR bands due to the $OH_{v+\delta}$ combination vibration are observed near 4530 cm^{-1} (2.20 μm) for montmorillonite, 4370 cm^{-1} (2.29 μm) for nontronite, and a doublet near 4340 cm^{-1} (2.3 μm) plus another weak band near 4190 cm^{-1} (2.39 μm) for hectorite (e.g. Clark *et al*., 1990; Bishop *et al*., 1994, 1999).

METHODS

Samples

Lizardite and chrysotile samples were selected from the suites used in the Mössbauer studies of O'Hanley & Dyar (1993, 1998); full details of the compositions, assemblages and geological settings are included in those papers. Samples include lizardite, chrysotile and picrolite (a field term for apple-green serpentine, which is chrysotile in the samples studied) from the Cassiar, Jeffrey and Woodsreef chrysotile asbestos deposits. All mineral separates were removed from billets using thin-sections to guide the areas to be drilled. Each was characterized by XRD, electron microprobe, Mössbauer, and uranium extraction (for H_2O). Samples were selected for this study to show a range in octahedral and tetrahedral cation compositions, as given in Table 1.

Smectite spectra were also selected for analysis here from previously studied samples.

TABLE 1. Cation compositions of smectites and serpentines in this study.

Sample	Octahedral cations Al	Fe^{3+}	Fe^{2+}	Li/Cr	Mg	Tetrahedral cations Si	Al	Fe^{3+}	Ref.
Smectites									
Appersdorf	2.79	0.48			0.83	7.99	0.01		@
Gossendorf	1.74	1.62			0.52	7.98	0.02		@
Manito	0.42	3.42	0.18		0.08	6.98	1.02		º
JP	2.99	0.38			0.63	7.70	0.30		#
Sampor	0.09	3.91			7.03	0.61	0.36		@
Sauteloup	2.78	0.70	0.04		0.52	7.70	0.30		º
SAz-1	2.67	0.15			1.20	8.00			†
Steinegg	0.25	2.84			0.98	7.97	0.03	0.83	@
SWy-1	3.07	0.44			0.54	7.66	0.34		#
Hector	0.01	0.01		0.62	4.76	7.99	0.01		^
Serpentines									
C54 chrysotile	0.22	0.09	0.09	0.00	5.61	3.80	0.16	0.04	+
C53 lizardite	0.09	0.08	0.04	0.06	5.80	3.77	0.09	0.14	*
J68 chrysotile	0.04	0.08	0.04	0.00	5.87	3.87	0.13	0.00	+
W15 chrysotile	0.27	0.00	0.22	0.00	5.46	3.86	0.08	0.06	+
W15 picrolite	0.16	0.05	0.17	0.01	5.50	3.88	0.10	0.02	+
W54 chrysotile	0.27	0.00	0.17	0.00	5.57	3.78	0.14	0.08	+

Li is present in the octahedral sheet for hectorite and Cr is present for some serpentines
@ data from Bishop *et al*. (2002); º data from Köster *et al*. (1999); # data from Madejová *et al*. (1994); † data from Breen *et al.* (1995); ^ data from Komadel *et al*. (1996); + data from O'Hanley and Dyar (1998); * data from O'Hanley and Dyar (1993)

Montmorillonites from Appersdorf, Germany (Bishop *et al*., 2002) and from Jelšový Potok (JP), Slovakia (Madejová *et al*., 1994), nontronites from Gossendorf, Austria, (Bishop *et al*., 2002), Sampor, Slovakia (Bishop *et al*., 1999), Manito, USA, and Sauteloup, France, (Köster *et al*., 1999) and a hectorite from Hector, California, USA (Komadel *et al*., 1996) were all prepared and analysed in previous studies and the octahedral and tetrahedral cation compositions are given in Table 1. Both the KGa-1 kaolinite, and the SAz-1 and SWy-1 montmorillonites were obtained from the Clay Minerals Society, Source Clays Repository.

Spectroscopic measurements

Transmittance spectra were measured on KBr pellets using a Nicolet Magna 550 Fourier-transform spectrometer and standard techniques as in other studies (Murad & Bishop, 2000; Bishop *et al*., 1999). Visible/near-infrared (NIR) reflectance spectra were measured on bulk powders in a horizontal position using both a bidirectional spectrometer (measured relative to Halon and corrected for absolute reflectance) and a Nicolet 740 Fourier-transform spectrometer (measured relative to a rough gold surface in a H_2O- and CO_2-purged environment) as described previously (Bishop *et al*., 1999).

Polarizing power determination

The influence that the octahedral and tetrahedral cations in phyllosilicates have on the OH-stretching and bending vibrations depends on the polarizing power of the cation, or its ability to withdraw electrons away from the hydroxyl group. A simple way to estimate this effect is to calculate the charge per radius of each cation based on the effective ionic radii (Huheey *et al*., 1993). This is given in Table 2 for the octahedral and tetrahedral cations frequently found in phyllosilicates.

RESULTS

Structural OH-stretching vibrations in serpentine-kaolin minerals

Transmittance spectra of the OH_v vibrations are shown in Fig. 1 for kaolinite and trioctahedral

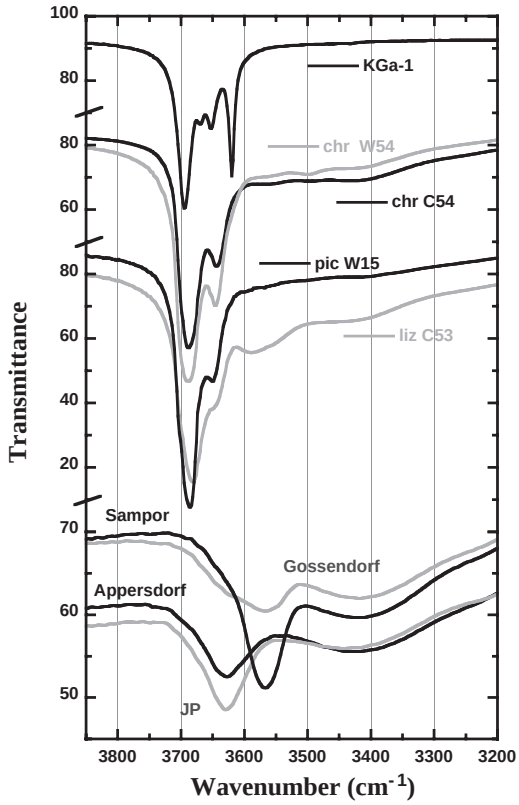

FIG. 1. Transmittance spectra of the OH-stretching bands for kaolinite (KGa-1), the serpentines chrysotile, lizardite and picrolite, the montmorillonites JP and Appersdorf, and the nontronites Sampor and Gossendorf.

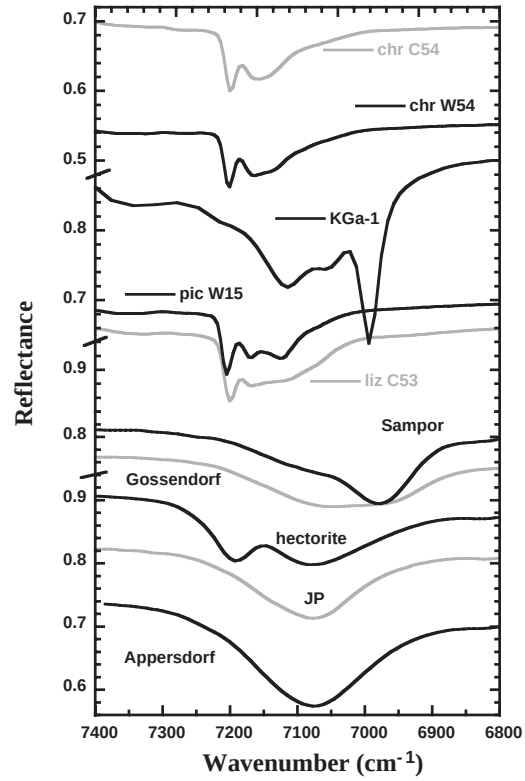

FIG. 2. Reflectance spectra of the OH-stretching overtone bands for kaolinite (KGa-1), the serpentines chrysotile, lizardite and picrolite, and the smectites JP, Appersdorf, hectorite, Sampor and Gossendorf.

serpentines and reflectance spectra of the corresponding overtone bands are shown in Fig. 2. Band centres determined from second derivatives are listed in Table 3. The vibrational energy of the overtone band is not simply twice the original band, but is somewhat less as explained by quantum mechanics. Comparison of the band centres for the mid-IR OH_v absorptions and NIR overtones for the serpentines in this study showed that a factor of 1.96 gave consistent results. The dominant OH_v band for the serpentines in this study was observed in Fig. 1 at 3689 cm^{-1} (chrysotile), 3682 cm^{-1} (lizardite) or 3685 cm^{-1} (picrolite) and the strongest OH_v overtone for these samples was observed in Fig. 2, at 7230, 7230 and 7240 cm^{-1}, respectively. Calculating these OH_v overtone bands using a factor of 1.96 gives 7230, 7217 and 7223 cm^{-1}, respectively, which compare well with

TABLE 2. Polarizing power of cations.

Cation	Coord	*R* (Å)	Charge	Ch/rad
Si	4	0.400	4	10.00
Al	4	0.530	3	5.66
Al	6	0.675	3	4.44
Fe	4	0.630	3	4.76
Fe	6	0.690	3	4.35
Fe	4	0.770	2	2.60
Fe	6	0.750	2	2.67
Mg	4	0.710	2	2.82
Mg	6	0.860	2	2.33
Cr	6	0.870	2	2.30
Li	6	0.900	1	1.11

Coord indicates tetrahedral or octahedral coordination; *R* is the effective ionic radius, from Huheey *et al.* (1993); Ch/rad is the charge per radius

the measured values (Table 3). This overtone factor has been used for calculating spectral features for the remaining samples.

For kaolinite KGa-1, the OH_ν absorptions are observed at 3622, 3653, 3672 and 3697 cm^{-1} (Fig. 1). A sharp OH_ν overtone was measured near 7069 cm^{-1} and broader bands were measured at 7232, 7175 and 7124 cm^{-1} (Fig. 2). Simple overtone calculation of the strongest bands at 3622 and 3697 cm^{-1} using a factor of 1.96 gives energies of 7099 and 7246 cm^{-1} that correspond roughly to the upper and lower bands observed in the NIR region. Calculating overtones by combining any two of the observed OH_ν vibrations gives values between 7130 and 7222 cm^{-1}. The shape of the NIR feature for KGa-1 is consistent with interactions occurring between the OH_ν bands at 3653, 3672 and 3697 cm^{-1}, supporting previous explanations of these bands (Farmer, 1998). A weak, broad band centred near 7350 cm^{-1} in the KGa-1 spectrum (Fig. 2) is attributed to a small amount of Si-OH. The overtone of Si-OH-stretching vibrations has been observed in this region and the Si-OH-bending vibration is found near 800 cm^{-1} (Anderson & Wickersheim, 1964).

Structural OH-combination bands in serpentines and smectites

Transmittance spectra of the OH_δ vibrations are shown in Fig. 3 and reflectance spectra of the $OH_{\nu+\delta}$ are shown in Fig. 4. Band centres determined from second derivatives are listed in Table 3. A doublet is observed in Fig. 3 for $OH_{\nu+\delta}$ in spectra of kaolinite centred near 4530 and 4633 cm^{-1} and weaker bands are observed from ~4195 to 4315 cm^{-1}. Multiple bands from 4080 to 4330 cm^{-1} are observed for the serpentine clay minerals, dominated by a strong doublet near 4270 and 4300 cm^{-1}. The primary OH combination band is observed near 4510 cm^{-1} for montmorillonite, near 4350 cm^{-1} for nontronite and near 4335 cm^{-1} for hectorite. Additional, weaker bands near 4080 and 4150–4200 cm^{-1} for Fe-bearing and Al-bearing smectites, respectively, have been observed for samples that also have bands in the 600–700 cm^{-1} region in a related study of a large group of smectites (Bishop *et al*., 2002). The NIR spectra of hectorite also contain weaker bands in this region centred at 4104 and 4195 cm^{-1}. Because these bands near 4080–4100 cm^{-1} and 4150–4200 cm^{-1} occur in the OH combination band region for phyllosilicates, potential fundamental $OH_{\nu'}$ and $OH_{\delta'}$ bands are investigated here for smectites that could explain these features as additional $OH_{\nu+\delta}$ combination bands for a minority of the OH sites.

The OH-bending vibrations for chrysotile are centred at 606 cm^{-1}, for lizardite at 625 cm^{-1}, and for picrolite at 611 cm^{-1}. Kaolinite KGa-1 exhibits band centres near 941, 915, 755 and 701 cm^{-1} which have been attributed to OH_δ (Farmer, 1974). Spectra of the nontronites from Sampor (data from Bishop *et al*., 1999) and Manito (data from Köster *et al*., 1999) in Fig. 4 contain the well known OH_δ

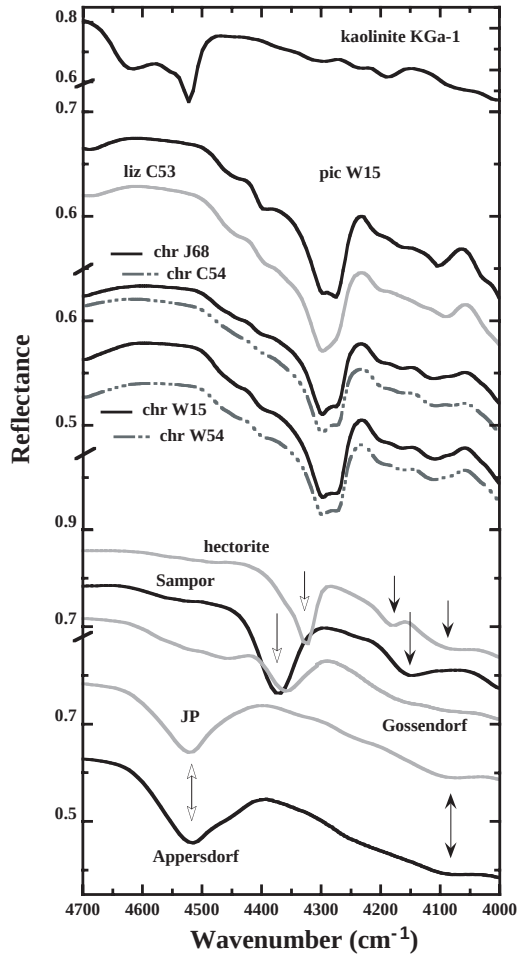

FIG. 3. Reflectance spectra of the OH-combination bands from 4000 to 4700 cm^{-1} for kaolinite, the serpentines: chrysotile, lizardite and picrolite, and the smectites: Ješový Potok (JP), Appersdorf, hectorite, Sampor and Gossendorf.

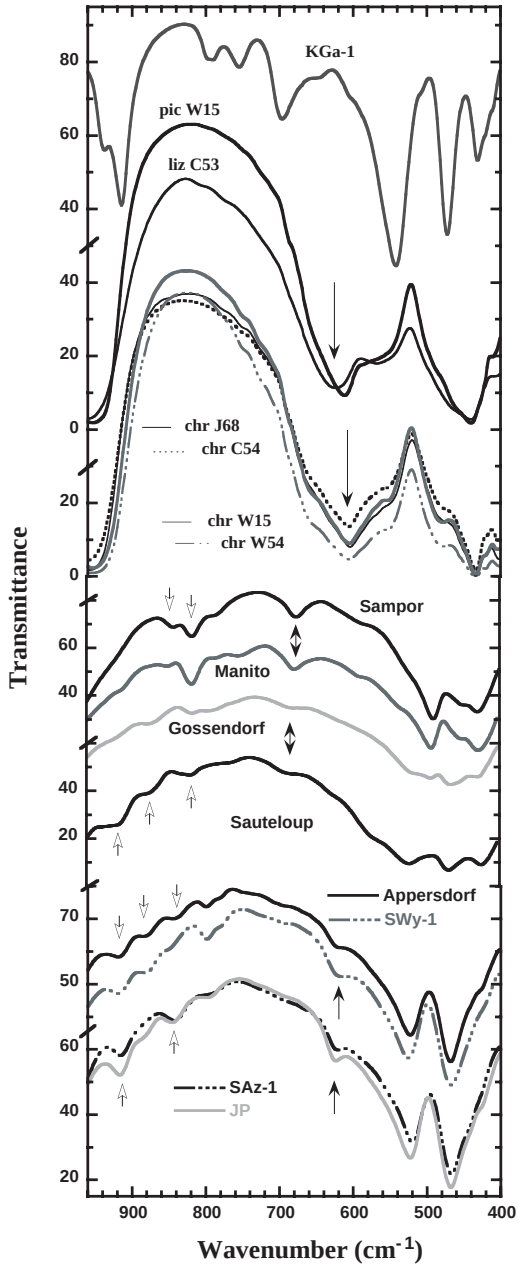

FIG. 4. Transmittance spectra of the OH-bending region from 400 to 960 cm^{-1} for kaolinite, serpentines (chrysotile, lizardite, picrolite), nontronites from Sampor and Manito, Fe-smectites Gossendorf and Sauteloup, and montmorillonites from SWy-1, Appersdorf, SAz-1 and Ješový Potok (JP).

absorption bands from 785 to 850 cm^{-1}, plus an additional band near 680 cm^{-1}. Spectra of Fe-bearing smectites from Gossendorf (data from Bishop *et al*., 2002) and Sauteloup (data from Köster *et al*., 1999) in Fig. 4 contain weaker OH_δ bands from 785 to 915 cm^{-1} as well as broadened, weaker bands near 680 cm^{-1}. Spectra of montmorillonites with the Wyoming and Cheto structures (data from Bishop *et al*., 2002) are also shown in Fig. 4 and exhibit the characteristic OH_δ vibrations in the 800–915 cm^{-1} region for these structures. These montmorillonite spectra also contain a band near 630 cm^{-1}.

In some earlier studies, spectral bands in the range 600–770 cm^{-1} for phyllosilicates were attributed to Si-O vibrations (Stubican & Roy, 1961b), then were later assigned to OH_δ in trioctahedral sheet silicates (e.g. Farmer, 1974) and were largely unnoticed for dioctahedral smectites. Liese (1967) found that a band near 670 cm^{-1} in IR spectra of biotites shifted to two bands near 660 and 715 cm^{-1} as the Fe^{2+} and Fe^{3+} contents increased and he further suggested that tetrahedral substitution may be involved. Hayashi & Oinuma (1965) found up to three bands in the range 600–770 cm^{-1} in IR spectra of highly substituted chlorites and noted that the vibrational energies of these bands were sensitive to the abundance of Al, Mg and Fe in octahedral positions. More recently, bands near 630 and 680 cm^{-1} have been observed for some montmorillonites and nontronites (e.g. Farmer, 1974; Goodman *et al*., 1976) and they have been shown to be associated with the octahedral cations through acid dissolution studies (Madejová *et al*., 1990).

For dioctahedral phyllosilicates the OH groups are tilted at 12–16° out of the cleavage plane and the proton is closer than usual to two of the O atoms on the tetrahedral apices (Farmer, 1974). Because of this configuration, dioctahedral smectites are particularly sensitive to tetrahedral substitution. Tetrahedral substitution of Al or Fe for Si disrupts the dioctahedral structure due to changes in cation size and charge (Table 2) that is compensated by substitution (charge compensation) or deprotonation in the adjacent octahedral layer. Deprotonation of smectites through internal oxidation-reduction reactions is described by Burt (1989) and Burns (1993) and may occur as a result of internal charge imbalances in the structure. Komadel *et al*. (1995) found that reduced and reoxidized nontronite contained 15–20% fewer OH sites, than did the original nontronite, based on changes in the IR bands. The charge per radius for

Si in tetrahedral sites is estimated at 10, while this value decreases to 5.7 for Al and 4.8 for Fe^{3+} (Table 2). Mg and Fe^{2+} are not commonly observed in these sites because the low charge per radius value of 2.8 would perturb the structure to a much greater extent.

Based on their polarizing powers, Fe^{3+} is not significantly less favoured than Al for tetrahedral sites, suggesting that tetrahedral Fe^{3+} substitution in sheet silicates may be more common than frequently considered. Besson & Drits (1997) have made similar arguments in favour of tetrahedral Fe^{3+} in smectites based on quantitative IR studies of OH-stretching vibrations. Goodman *et al*. (1976) also suggested higher abundances of tetrahedral Fe^{3+} in nontronites than would be present if Al is preferentially assigned to these sites.

Charge compensation may also be accompanied by *M*1 site occupancy, creating pockets of trioctahedral-like structure and/or H-bonding between the hydroxyls and the apical O atoms with residual negative charge. Farmer (1974) employed these arguments to explain lowered OH-stretching vibrations (weakened OH bonds) in tetrahedrally-substituted phyllosilicates and stated that similar trends are expected for samples with high octahedral substitution as well. Comparing the charge per radius values from Table 2 for octahedrally configured cations shows ~4.4 for both Al and Fe^{3+}, whereas much lower values are observed for Fe^{2+}, Mg and Cr. This suggests that little structural change will result from exchanging Al and Fe^{3+} in octahedral sites, but that significant steric changes are expected when Fe^{2+}, Mg or Cr occupy octahedral sites. Manceau *et al*. (2000) suggest that octahedral cations are not distributed randomly in smectites, rather that pockets of trioctahedral Fe^{2+} clusters are observed in reduced dioctahedral smectites. They found a change in the OH_ν band observed at 3570 cm^{-1} for nontronite to two bands at 3530 and 3623 cm^{-1} for reduced nontronite, and Fialips *et al*. (2001) observed that the bands at 823 and 843 cm^{-1} in spectra of Garfield nontronite were replaced by a band at 656 cm^{-1} in spectra of the reduced sample.

Naturally-occurring micas frequently exhibit compositions in between dioctahedral and trioctahedral (Bailey, 1980). This may be inherent in the composition of the assemblage, or it may be caused by loss of OH for charge balance. H measurements for serpentines in recent studies showed lower than stoichiometric values (e.g. O'Hanley & Dyar, 1993, 1998). When an OH site is vacant, the adjacent OH must move. This effect combined with structural perturbations due to some trioctahedral substitution into the dioctahedral compositions and of divalent substitution into nominally trivalent sites probably contributes to changes in the IR spectral absorptions.

Farmer (1974) noted that celadonite and montmorillonite have many similar OH-bending and stretching bands though celadonite has an additional out-of-plane $MgFe^{3+}OH$-bending vibration near 680 cm^{-1} that has not previously been reported for montmorillonite and a markedly lower AlMgOH-stretching frequency compared to that of montmorillonite. Perhaps the unusual $M^{2+}M^{3+}$ dioctahedral combination in celadonite (Wise & Eugster, 1964) provides a structural perturbation that allows this OH_δ band, typically observed for trioctahedral, but not dioctahedral, sheet silicates to form. A similar argument can be applied to dioctahedral smectites, such that if the structure is sufficiently perturbed through extensive tetrahedral or octahedral substitution or pockets of trioctahedral character, then weak out-of-plane OH-bending vibrations in the range 600–700 cm^{-1} are observed. In order to test this hypothesis the potential out-of-plane bending vibrations ($OH_{\delta'}$) are listed in Table 3 and are compared with the NIR region combination and overtone bands.

Combination bands ($OH_{\nu+\delta}$) were first calculated using the dominant OH_ν and OH_δ bands, which gives consistent results (e.g. 4386 cm^{-1} *vs.* 4380 cm^{-1} for Sampor, 4550 and 4512 cm^{-1} *vs.* 4535 cm^{-1} for SWy-1, see Table 3). The exact OH_ν values are difficult to determine because of multiple overlapping bands here due to several M_1M_2OH sites, as well as water-stretching vibrations. Some OH_ν bands were estimated from the measured $OH_{\nu+\delta}$ and OH_δ bands and are listed on the left side of Table 3 for the smectites. Overtones of these calculated OH_ν bands (6980 cm^{-1} Sampor, 7056 cm^{-1} SWa-1, 7076 cm^{-1} JP, 7093 cm^{-1} SWy-1, 7213 cm^{-1} for hectorite) match well with the measured OH_ν overtones. This technique is still an approximation because of the multiple M_1M_2OH sites, although the H_2O bands are not interfering. A more precise approach would be to combine the individual $M_1M_2OH_\nu$ and $M_1M_2OH_\delta$ bands. This is beyond the scope of the current study.

Combination bands were next tested using the proposed out-of-plane OH_δ bands near 630 and 680 cm^{-1}, for montmorillonite and nontronite, respectively. Farmer (1974) suggested that OH_ν is

TABLE 3. Summary of IR bands.

	Calculated				Measured					
	1.96*OH_ν		$OH_{\nu+\delta,\ \delta'}$		OT OH_ν	$OH_{\nu+\delta,\ \delta'}$		OH_ν	OH_δ	$OH_{\delta'}$
Kaolinite										
KGa-1	**7246** (1)	**7222** (1,2)	**4638** (1+5)	4249 (3494+7)	**7232**	**4633**	4312	**3697** (1)	**941** (5)	**755** (7)
	7173 (1,4)	**7203** (1,3)	**4537** (4+6)	4195 (3494+8)	**7175**	**4530**	4250	**3672** (2)	**915** (6)	**701** (8)
		7148 (2,4)			**7124**		4195	**3653** (3)		
	7099 (4)	**7130** (3,4)			**7069**			**3622** (4)		
Serpentine										
Chrysotile	**7230** (1)		**4295** (1+4)	4332 (1,2+3)	**7230**	**4297**	4324	**3689** (1)		~665 (3)
C54 & J68	**7186** (1,2)		**4250** (2+4)	4212 (1,2+5)	~7200	**4270**	4205	**3644** (2)		**606** (4)
	7142 (2)			4166 (3590+4,5)	**7185**		4165			~545 (5)
					~7160					
Chrysotile	**7230** (1)		**4295** (1+5)	4326 (1,2+4)	**7230**	**4297**	4324	**3689** (1)		~658 (4)
W15 & W54	**7188** (1,2)		**4252** (2+5)	4218 (1,2+6)	**7205**	**4270**	4208	**3646** (2)		**606** (5)
	7146 (2)			4168 (3590+4,5)	~7180		4165	3496 (3)		~550 (6)
				4074 (3+5,6)	~7160		4105			
Lizardite	**7217** (1)		**4307** (1+7)	4331 (1,2+6)	**7230**	**4301**	4335	**3682** (1)	731 (4)	~665 (6)
C53	**7185** (1,2)		**4275** (2+7)	4222 (1,2+8,9)	**7205**	**4270**	4205	**3650** (2)	754 (5)	**625** (7)
	7154 (2)			4169 (3,3500+7)	~7160		4085	3588 (3)		~569 (8)
				4056 (3500+8,9)	~7120					~543 (9)
Picrolite	**7223** (1)		**4296** (1+6)	4326 (1,2+5)	**7240**	**4301**	4332	**3685** (1)	731 (3)	**~658** (5)
W15	**7189** (1,2)		**4262** (2+6)	4211 (1,2+7)	**7210**	**4270**	4212	**3651** (2)	754 (4)	**611** (6)
	7156 (2)			4197 (3620+6,7)	**7170**		4168			~543 (7)
				4077 (3500+6,7)	~7150		4105			

TABLE 3 (contd.)

	Calculated				Measured					
	1.96*OH_ν	$OH_{\nu+\delta}$	$OH_{\nu+\delta'}$	OH_ν	OT OH_ν	$OH_{\nu+\delta}$	$OH_{\nu+\delta'}$	OH_ν	OH_δ	$OH_{\delta'}$
Nontronite										
Sampor	**6991** (1)	**6980** (11)	**4386** (1+3)	**4169** (11-70+5)	**3561** (11, 8-3)	**6980** (9)	~4575 (7)	**4165** (6)	**3567** (1)	**845** (2)	**678** (5)
		6835 (12)		**4175** (1-70+5)	**3487** (12, 6-5)	**6820** (10)	**4380** (8)			**819** (3)	
										~785 (4)	
SWa-1	**6997** (1)	**7056** (13)	**4445** (1+2)		**3600** (13, 8-2)	**7090** (10)	~4575 (7)	**4170** (6)	**3570** (1)	**875** (2)	**681** (5)
		6972 (14)	**4388** (1+3)	**4168** (14-70+5)	**3557** (14, 9-3)	**6970** (11)	**4475** (8)			**818** (3)	
		6838 (15)		**4181** (1-70+5)	**3489** (15, 6-5)	**6820** (12)	**4375** (9)			**784** (4)	
Montmorillonite											
JP	**7113** (1)	**7076** (9)	**4544** (1+2)	**4169** (9-70+4)	**3610** (9, 6-2)	**7070** (7)	**4525** (6)	**4105** (5)	**3629** (1)	**915** (2)	**629** (4)
		6813 (10)	**4512** (1+3)	**4188** (1-70+4)	**3476** (10, 5-4)	**6820** (8)				**883** (3)	
SWy-1	**7123** (1)	**7093** (9)	**4550** (1+2)	**4176** (9-70+4)	**3619** (9, 6-2)	**7090** (7)	**4535** (6)	**4090** (5)	**3634** (1)	**916** (2)	**627** (4)
		6787 (10)	**4512** (1+3)	**4191** (1-70+4)	**3463** (10, 5-4)	**6820** (8)				**878** (3)	
Hectorite	**7217** (1)	**7213** (11)	**4337** (1+4)		**3680** (11, 7-4)	**7202** (8)	**4335** (7)	**4195** (5)	**3682** (1)		**655** (4)
	7152 (2)	**6938** (12)	**4304** (2+4)		**3540** (12, 5-4)	**7095** (9)		**4104** (6)	**3649** (2)		
	6723 (3)	**6760** (13)	**4085** (3+4)		**3449** (13, 6-4)	**6820** (10)			~3430 (3)		

All vibrations are given in cm^{-1} and boldface type indicates a strong band; numbers in () to the right of measured vibrations are used for identification of the calculated bands (i.e. 1+2 or 5−4), where only underlined values are numbers rather than references and in some cases two sets of combinations are averaged (i.e. 1,2+5 indicates an average of 1+5 and 2+5); OT indicates overtone of specified vibration.

lowered due to H bonding by at least 40 cm^{-1} for highly substituted smectites. Russell & Farmer (1964) observed a shift in OH_ν from 3629 cm^{-1} to a main band at 3530 cm^{-1} and the appearance of a new narrow doublet near 3640–3655 cm^{-1} in spectra of disrupted montmorillonites. Combining the measured OH_ν minus 70 cm^{-1} and the $OH_{\delta'}$ bands gives values similar to the new (possible $OH_{\nu+\delta'}$) bands in the NIR combination region for nontronites with tetrahedral substitution (e.g. Sampor). This should hold as well for highly substituted montmorillonites. However, an offset of 70 cm^{-1} does not match well (4170 cm^{-1} *vs.* 4100 cm^{-1}). Perhaps the OH_ν band for substituted montmorillonite is lowered more than in the nontronite case. Another approach was also taken to evaluate these bands near 4000–4200 cm^{-1}. New OH_ν bands were calculated for the dioctahedral smectites by subtracting the $OH_{\delta'}$ bands from the potential $OH_{\nu+\delta'}$ bands near 4170 and 4100 cm^{-1}. These values are also listed as OH_ν on the calculated side of Table 3. The overtones of these OH_ν bands are 6835 cm^{-1} for Sampor, 6838 cm^{-1} for SWa-1, 6813 cm^{-1} for JP, and 6787 cm^{-1} for SWy-1, which correspond well with weak observed overtone bands.

Calculations were also performed to explain the $OH_{\nu+\delta}$ and OH_δ bands in serpentine-kaolin minerals. Weak bands in the OH combination region of the serpentine and kaolinite reflectance spectra are observed near 4100–4300 cm^{-1} (Table 3) and can be explained through combinations of the measured OH_ν and OH_δ values. The calculated combination bands are listed on the left side of Table 3 and include averages of two related bands in some cases. Additional weak bands above 4300 cm^{-1} in serpentine spectra can be explained by a combination of OH_ν plus an OH_δ band in the 700–800 cm^{-1} range. Weak bands are observed as shoulders in the serpentine spectra but can be identified as peaks at 731 and 754 cm^{-1} in the second derivative spectra. Combining these bands with an average of the two OH_ν bands gives very good agreement with the observed bands near 4325–4335 cm^{-1}. Additional possible combination bands were calculated from measured and estimated OH_ν bands and measured OH_δ bands that may explain the weak features observed in NIR serpentine spectra from ~4100–4200 cm^{-1}. These are reported in Table 3.

For kaolinite, combination bands are calculated at 4537 and 4638 cm^{-1} from the two strongest OH_ν bands and two of the OH_δ bands. These values compare well with the measured values of 4530 and 4633 cm^{-1} for $OH_{\nu+\delta}$ suggesting that the OH_ν band at 3697 cm^{-1} and OH_δ band at 941 cm^{-1} are associated and that the OH_ν band at 3622 cm^{-1} and OH_δ band at 915 cm^{-1} are related. Additional calculations were made using the OH_δ bands observed at 701 and 755 cm^{-1}. An OH_ν band value of 3494 cm^{-1} was found to give calculated $OH_{\nu+\delta}$ values of 4195 and 4249, very close to the measured values of weaker NIR bands for KGa-1, although no OH_ν band value of 3494 cm^{-1} was observed in the spectra of KGa-1.

CONCLUSIONS

Analysis of the mid-IR fundamental stretching and bending vibrations for structural OH in phyllosilicates, together with the NIR spectral overtones and combinations, enables testing of band assignments for the structural OH vibrations. The spectral analyses of selected samples of smectites and serpentine-kaolin minerals here suggest the following conclusions. (1) The bands centred near 680 cm^{-1} in some Fe-rich smectites and near 630 cm^{-1} in some Al-rich smectites are assigned to OH bending when the structure is disrupted by (a) higher than usual tetrahedral substitution of Fe^{3+} or Al for Si and/or octahedral cation substitution, and/or (b) variations in hydroxyl position due to missing OH groups. These may be the out-of-plane bending vibrations predicted by Farmer (1974) and may represent small pockets of trioctahedral character within the dioctahedral smectite structure. (2) Kaolinite exhibits OH-bending vibrations in both the in-plane and out-of-plane regions for phyllosilicates. The OH-bending vibrations for chrysotile and lizardite occur near 605–625 cm^{-1} and may be best explained by out-of-plane vibrations because of the disrupted structure in serpentines. Weak features near 730 and 750 cm^{-1} are observed in the serpentine spectra in this study and correspond with weak OH combination features in the NIR region, suggesting that these may also be OH-bending vibrations. (3) Spectral analyses indicate that the 3620 cm^{-1} OH-stretching overtone is strong and sharp for kaolinite, suggesting that little interaction with other OH-stretching vibrations occurs, while the overtone of the 3697 cm^{-1} band is greatly broadened, which is consistent with the resonance explanations for the bands at 3653 and 3672 cm^{-1}.

ACKNOWLEDGMENTS

Reflectance spectra were measured at RELAB, a multi-user, NASA-supported facility (NAG5-3871) at Brown University. Assistance from T. Hiroi with the bi-directional spectra is much appreciated. MDD acknowledges support from NASA grant NAG5-10424. This paper has benefited from the helpful comments of J. Madejová and an anonymous reviewer.

REFERENCES

Anderson J.H. & Wickersheim K.A. (1964) Near infrared characterization of water and hydroxyl groups on silica surfaces. *Surface Science*, **2**, 252–260.

Bailey S.W. (1980) Structures of layer silicates. Pp. 1–124 in: *Crystal Structures of Clay Minerals and their X-ray Identification* (G.W. Brindley & G. Brown, editors). Monograph **5**, Mineralogical Society, London.

Bell J.F., III (1996) Iron, sulfate, carbonate, and hydrated minerals on Mars. Pp. 359–380 in: *Mineral Spectroscopy: A tribute to Roger G. Burns* (M.D. Dyar, C. McCammon & M.W. Schaefer, editors). The Geochemical Society, Houston, Texas, USA.

Besson G. & Drits V.A. (1997) Refined relationships between chemical composition of dioctahedral fine-grained micaceous minerals and their infrared spectra within the OH stretching region. Part II: The main factors affecting OH vibrations and quantitative analysis. *Clays and Clay Minerals*, **45**, 170–183.

Bish D. (1993) Rietveld refinement of the kaolinite structure at 1.5 K. *Clays and Clay Minerals*, **41**, 738–744.

Bishop J.L. & Murad E. (1996) Schwertmannite on Mars? Spectroscopic analyses of schwertmannite, its relationship to other ferric minerals, and its possible presence in the surface material on Mars. Pp. 337–358 in: *Mineral Spectroscopy: A tribute to Roger G. Burns* (M.D. Dyar, C. McCammon & M.W. Schaefer, editors). The Geochemical Society, Houston, Texas, USA.

Bishop J.L., Pieters C.M. & Edwards J.O. (1994) Infrared spectroscopic analyses on the nature of water in montmorillonite. *Clays and Clay Minerals*, **42**, 701–715.

Bishop J.L., Murad E., Madejová J., Komadel P., Wagner U. & Scheinost A. (1999) Visible, Mössbauer and infrared spectroscopy of dioctahedral smectites: Structural analyses of the Fe-bearing smectites Sampor, SWy-1 and SWa-1. Pp. 413–419 in: *11th International Clay Conference, June, 1997*.

Bishop J.L., Schiffman P. & Southard R.J. (2001) Geochemical and mineralogical analyses of palagonitic tuffs and altered rinds of pillow lavas on Iceland and applications to Mars. Pp. 371-392 in: *Volcano-Ice Interaction on Earth and Mars* (J.L. Smellie and M.G. Chapman, editors). Special Publication, **202**, Geological Society, London.

Bishop J.L., Madejová J., Komadel P. & Froeschl H. (2002) The influence of structural Fe, Al and Mg on the infrared OH bands in spectra of dioctahedral smectites. *Clay Minerals*, **37**, 607–616.

Breen C., Madejová J. & Komadel P. (1995) Characterisation of moderately acid-treated, size-fractionated montmorillonites using IR and MAS NMR spectroscopy and thermal analysis. *Journal of Material Chemistry*, **5**, 469–474.

Burns R.G. (1993) Rates and mechanisms of chemical weathering of ferromagnesian silicate minerals on Mars. *Geochimica et Cosmochimica Acta*, **57**, 4555–4574.

Burt D.M. (1989) Iron-rich minerals on Mars: Potential sources or sinks for hydrogen and indicators of hydrogen loss over time. Pp. 423–432 in: *19th Lunar and Planetary Science Conference*.

Clark R.N., King T.V.V., Klejwa M. & Swayze G.A. (1990) High spectral resolution reflectance spectroscopy of minerals. *Journal of Geophysical Research*, **95**, 12653–12680.

Cornell R.M. & Schwertmann U. (1996) *The Iron Oxides*. VCH, New York.

Farmer V.C. (1974) The layer silicates. Pp. 331–363 in: *The Infrared Spectra of Minerals* (V.C. Farmer, editor). Monograph **4**, The Mineralogical Society, London.

Farmer V.C. (1998) Differing effects of particle size and shape in the infrared and Raman spectra of kaolinite. *Clay Minerals*, **33**, 601–604.

Fialips C.-I., Huo D., Yan L., Wu J. & Stucki J.W. (2001) Effect of iron oxidation state on the IR spectra of Garfield nontronite. *American Mineralogist*, **86**, 630–641.

Goodman B.A., Russell J.D., Fraser A.R. & Woodhams F.W.D. (1976) A Mössbauer and IR spectroscopy study of the structure of nontronite. *Clays and Clay Minerals*, **24**, 53–59.

Hayashi H. & Oinuma K. (1965) Relationship between infrared absorption spectra in the region of 450–900 cm^{-1} and chemical composition of chlorite. *American Mineralogist*, **50**, 476–483.

Huheey J.E., Keiter E.A. & Keiter R.L. (1993) *Inorganic Chemistry. Principles of Structure and Reactivity*. Harper Collins, New York.

King T.V.V. & Clark R.N. (1989) Spectral characteristics of chlorites and Mg-serpentines using high-resolution reflectance spectroscopy. *Journal of Geophysical Research*, **94**, 13,997–14,008.

Komadel P., Madejová J. & Stucki J.W. (1995) Reduction and reoxidation of nontronite: Questions

of reversibility. *Clays and Clay Minerals*, **43**, 105–110.

Komadel P., Madejová J., Janek M., Gates W.P., Kirkpatrick R.J. & Stucki J.W. (1996) Dissolution of hectorite in inorganic acids. *Clays and Clay Minerals*, **44**, 228–236.

Köster H.M., Ehrlicher U., Gilg H.A., Jordan R., Murad E. & Onnich K. (1999) Mineralogical and chemical characteristics of five nontronites and Fe-rich smectites. *Clay Minerals*, **34**, 579–599.

Liese H.C. (1967) Supplemental data on the correlation of infrared absorption spectra and composition in biotites. *American Mineralogist*, **52**, 877–880.

Madejová J., Bednáriková E., Komadel P. & Čičel B. (1990) Structural study of acid-treated smectites by IR spectroscopy. Pp. 267–271 in: *11th Conference on Clay Mineralogy and Petrology*.

Madejová J., Komadel P. & Čičel B. (1994) Infrared study of octahedral site populations in smectites. *Clay Minerals*, **29**, 319–326.

Manceau A., Drits V.A., Lanson B., Chateigner D., Wu J., Huo D., Gates W.P. & Stucki J.W. (2000) Oxidation-reduction mechanism of iron in dioctahedral smectites: II. Crystal chemistry of reduced Garfield nontronite. *American Mineralogist*, **85**, 153–172.

McSween H.Y., Jr. & Keil K. (2000) Mixing relationships in the Martian regolith and the composition of the globally homogeneous dust. *Geochimica Cosmochimica Acta*, **64**, 2155–2166.

Mendelovici E., Yariv S. & Villalba R. (1979) Iron-bearing kaolinite in Venezuelan laterites. 1. Infrared spectroscopy and chemical dissolution evidence. *Clay Minerals*, **14**, 323–331.

Murad E. & Bishop J.L. (2000) The infrared spectrum of synthetic akaganéite, ß-FeOOH. *American Mineralogist*, **85**, 716–721.

O'Hanley D.S. & Dyar M.D. (1993) The composition of lizardite 1*T* and the formation of magnetite in serpentines. *American Mineralogist*, **78**, 391–404.

O'Hanley D.S. & Dyar M.D. (1998) The composition of chrysotile and its relationship with lizardite. *The Canadian Mineralogist*, **36**, 727–739.

Russell J.D. & Farmer V.C. (1964) Infra-red spectroscopic study of the dehydration of montmorillonite and saponite. *Clay Minerals Bulletin*, **5**, 443–464.

Schwertmann U. & Cornell R.M. (2000) *Iron Oxides in the Laboratory*. Wiley-VCH, New York.

Stubican V. & Roy R. (1961a) A new approach to the assignment of infrared absorption bands in layer silicates. *Zeitschrift für Kristallographie*, **115**, 200–214.

Stubican V. & Roy R. (1961b) Isomorphous substitution and infra-red spectra of the layer lattice silicates. *American Mineralogist*, **46**, 32–51.

Vantelon D., Pelletier M., Barres O., Thomas F. & Michot L.J. (2001) Fe, Mg and Al distribution in the octahedral sheet of montmorillonites. An infrared study in the OH-bending region. *Clay Minerals*, **36**, 369 – 379.

Wise M.S. & Eugster H.P. (1964) Celadonite: Synthesis, thermal stability and occurrence. *American Mineralogist*, **49**, 1031–1083.